Elevated pyramidal cell firing orchestrates arteriolar vasoconstriction through COX-2-derived prostaglandin E2 signaling

B Le Gac[1], M Tournissac[2], Belzic E[1], S Picaud[1], I Dusart[1], H Soula[3], D Li[1], S Charpak[2], B Cauli[1*]

1. Sorbonne Université, CNRS, INSERM, Neurosciences Paris Seine - Institut de Biologie Paris Seine (NPS-IBPS), 9 quai Saint Bernard, 75005 Paris, France.

2. Sorbonne Université, INSERM, CNRS, Institut de la Vision, 17 rue Moreau, 75012 Paris, France.

3. Sorbonne Université, INSERM, Nutrition and Obesities: Systemic Approaches, NutriOmics, research unit, 91 boulevard de l'hôpital, 75013 Paris, France.

*Correspondence: bruno.cauli@upmc.fr

ABSTRACT

Neurovascular coupling (NVC), linking neuronal activity to cerebral blood flow (CBF), is essential for brain function and underpins functional brain imaging. Whereas mechanisms involved in vasodilation are well-documented, those controlling vasoconstriction remain overlooked. This study unravels the mechanisms by which pyramidal cells elicit arteriole vasoconstriction. Using patch-clamp recording, vascular and Ca^{2+} imaging in Emx1-Cre;Ai32 mouse cortical slices, we show that strong optogenetic activation of layer II/III pyramidal cells induces arteriole vasoconstriction, correlating with firing frequency and somatic Ca^{2+} increase. *Ex vivo* and *in vivo* pharmacological investigations indicate that this neurogenic vasoconstriction extends beyond glutamatergic transmission and predominantly recruits prostaglandin E2 (PGE2) through the cyclooxygenase-2 (COX-2) pathway, and activation of EP1 and EP3 receptors. Single-cell RT-PCR further identifies layer II/III pyramidal cells as a key source of COX-2-derived PGE2. Additionally, we present evidence that specific neuropeptide Y (NPY) interneurons acting on Y1 receptor, and astrocytes, through 20-hydroxyeicosatetraenoic acid (20-HETE) and COX-1-derived PGE2, contribute to this process. By revealing the mechanisms by which the activity of pyramidal cells leads to vasoconstriction, our findings shed light on the complex regulation of CBF.

Introduction

The brain critically depends on the uninterrupted blood supply provided by a dense vasculature[1]. Cerebral blood flow (CBF) is locally and temporally controlled by neuronal activity, this essential process is called neurovascular coupling (NVC), and is impaired in early stages of numerous neurological disorders[2]. NVC also serves as the physiological basis for functional brain imaging widely used to map neuronal activity. Increased neuronal activity increases CBF within seconds[2]. In the cerebral cortex, the hyperemic response linked to neural activity is supported by dynamically controlled vasodilation that is spatially and temporally restricted by delayed vasoconstriction in the surrounding area[3]. Conversely, vasoconstriction and decreased CBF usually correlate with reduced neuronal activity[3,4].

However, mounting evidence indicates that under physiological conditions the positive correlation between neuronal activity and CBF is not always met. For instance, i) robust sensory-evoked vasodilation can occur in the absence of substantial neuronal response[5], ii) conversely, pronounced neuronal activity is not systematically associated with increased hemodynamics[6], iii) CBF is decreased in several cortical areas despite local increase in neuronal activity[7] and iv) optogenetic simulation of inhibitory GABAergic interneurons results in vasodilation[8]. Furthermore, in pathological conditions with intense neuronal activity such as epileptic seizures, a sustained hypoperfusion/vasoconstriction is observed[9,10].

NVC is achieved by the synthesis and release of vasoactive messengers within the neurovascular unit[2], which act on the contractility of mural cells (smooth muscle cells and pericytes) to control vessel caliber and CBF along the vascular tree[11]. Pial and penetrating arterioles, which have a higher density of contractile mural cells and control their diameter faster than capillaries[11–14], play a key role in regulating CBF. Messengers of vasodilation released by excitatory neurons, GABAergic interneurons, astrocytes, or endothelial cells, include nitric oxide, K^+, arachidonic acid derivatives such as prostaglandin E2 (PGE2)[2], or more recently glutamate[15]. Despite its physio pathological importance, vasoconstriction is less understood with fewer cell types and vasoactive messengers that have been identified. It is now generally accepted that GABAergic interneurons are key players in vasoconstriction by releasing neuropeptide Y (NPY)[8,16]. However, under certain conditions astrocytes can also induce vasoconstriction via 20-hydroxyeicosatetraenoic acid (20-HETE)[17] or high K^+

concentration[18]. The involvement of pyramidal cells in the process remains to be investigated.

PGE2 has emerged as a bimodal messenger of NVC, similar to K^{+}[18] and glutamate[15], that can induce either vasodilation[19–22] or vasoconstriction[23,24] depending on its concentration and/or site of action along the vascular tree. Under physiological conditions, PGE2 is produced during NVC by either astrocytes[21] or pyramidal cells[22] via the rate-limiting synthesizing enzymes cyclooxygenase-1 (COX-1) or -2 (COX-2), respectively. Since COX-2-expressing pyramidal cells can release glutamate and PGE2, both of which induce vasoconstriction at high concentrations[15,23,24], pyramidal cells may be responsible for vasoconstriction when their spiking activity is high.

To test this hypothesis, we used *ex vivo* and *in vivo* approaches in combination with optogenetics to precisely control pyramidal cell firing in the mouse barrel cortex while monitoring the resulting arteriolar response. We found that pyramidal cells induce vasoconstriction at high stimulation frequency and express all the transcripts required for a cell autonomous synthesis of the vasoconstrictor messengers, PGE2 and prostaglandin F2α (PGF2α). Pharmacological investigations revealed that this neurogenic vasoconstriction depends on COX-2-derived PGE2 via the direct activation of vascular EP1 and EP3 receptors. It also involves the recruitment of intermediary NPY interneurons acting on the Y1 receptor, and, to a lesser extent astrocytes, via 20-HETE and COX-1-derived PGE2. Thus, our study reveals the mechanisms by which high frequency pyramidal cell firing leads to vasoconstriction.

Results

Pyramidal cells induce vasoconstriction at high firing frequency.

To determine if pyramidal cells action potential (AP) firing can induce vasoconstriction in a frequency-dependent manner, we used optogenetics to induce AP firing while monitoring the resulting vascular response in cortical slices. We used Emx1-cre;Ai32 transgenic mice expressing the H134R variant of channelrhodopsin-2 (ChR2) in the cortical glutamatergic neurons[25], conferring robust pyramidal cell photoexcitability[26]. Wide-field photostimulation of cortical slices was achieved in layers I to III (Supplementary Fig. 1a) using 10-second trains

77 of 5 ms light pulses (see Methods) delivered at five different frequencies (1, 2, 5, 10 and 20
78 Hz, Fig. 1a).

79 First, we ensured the efficiency of the photostimulation paradigm by recording layer II-III
80 pyramidal cells in whole-cell current clamp mode (Fig. 1a). We observed that optogenetic
81 stimulation resulted in the firing of an initial AP that was followed by a train of spikes whose
82 amplitude and frequency transiently decreased before reaching a steady state (Fig. 1a, upper
83 traces). Consistent with the kinetic properties of the H134R ChR2 variant[27] and the intrinsic
84 firing properties of pyramidal cells[28], the steady-state firing frequency matched the
85 photostimulation frequency up to 5 Hz but was lower at higher frequencies (Fig. 1a, steady-
86 state spike success rate: 100 ± 0 % at 1, 2 and 5 Hz, 70 ± 11 % at 10 Hz and 55 ± 12 % at 20
87 Hz). These observations demonstrate efficient pyramidal cell activation over a wide range of
88 photostimulation frequencies.

89 To test the prediction that neuronal activity induces vasoconstriction, we visualized the
90 optogenetically-induced response of penetrating arterioles. Layer I arterioles were imaged
91 for 30 minutes in cortical slices (Supplementary Fig.2; Supp. table 1) without preconstriction
92 to facilitate observation of vasoconstriction[16]. Examination of the evoked vascular response
93 over 30-minutes (Supplementary Fig.2) showed that increasing the frequency of
94 photostimulation shifted the overall vascular response from a barely discernible delayed
95 response between 1 Hz and 5 Hz to a sustained vasoconstriction at 10 Hz and above. This
96 tendency was particularly pronounced at 20 Hz, with most vessels (n= 8 of 10 arterioles)
97 showing a strong and rapid vasoconstriction. On average, this response peaked at 6.8 ± 2.4
98 min, much earlier than at lower frequencies, which typically required more than 10 min to
99 reach a maximum (Supplementary Fig.2c, 1 Hz: 15.6 ± 4.0 min; 2 Hz: 13.2 ± 2.3 min; 5 Hz:
100 16.0 ± 3.6 min; 10 Hz: 15.7 ± 2.4 min). Because the vascular response shifted to reliable
101 vasoconstriction in less than 10 minutes when the frequency of photostimulation was
102 increased to 20 Hz, we defined the first 10 minutes of recording as the vasoconstriction time
103 frame for subsequent comparisons and analyses. While photostimulation at 1 to 5 Hz failed
104 to elicit fast reliable vascular responses (Fig. 1c-d), 10 Hz photostimulation predominantly
105 induced vasoconstriction (n= 4 of 5 arterioles, Fig. 1 c-d, area under the curve (AUC)= -1.7 ±
106 1.1 x 10^3 %.s, n= 5). This response was even more pronounced at 20 Hz, as all arterioles
107 showed vasoconstriction of high magnitude (Fig. 1 b-d; AUC= -3.7 ± 0.7 x 10^3 %.s, $F_{(4, 30)}$=

108 6.135, p= 9.89 x 10^{-4}, one-way ANOVA, n= 10 arterioles). This difference was particularly
109 striking when comparing the magnitude at 20 Hz (Fig. 1d) with those at 1 Hz ($t_{(12)}$= -3.48, p=
110 0.0407, t-test), 2 Hz ($t_{(18)}$= -4.09, p= 0.0250, t-test) and 5 Hz ($t_{(14)}$= -3.7, p= 0.0346, t-test).
111 Intense optogenetic stimulation of pyramidal cells has been shown to elicit cortical
112 spreading depression[29], which induces vasoconstriction[15] and fast cell swelling[30]. We ruled
113 out this possibility by showing that the rate of change in light transmittance associated with
114 cell swelling remained below that of cortical spreading depression[30] (Supplementary Table
115 1). On the other hand, ChR2-independent vascular changes induced by high light intensity
116 have been reported[31]. We verified that 20 Hz photostimulation did not induce a vascular
117 response in wild-type mice that do not express ChR2 (Supplementary Fig.1). Taken together,
118 our observations indicate that photostimulation of pyramidal cells produces a frequency-
119 dependent vasoconstriction that occurs and amplifies at high firing rates.

120 **Optogenetic stimulation induces a frequency-dependent, gradual increase in somatic**
121 **calcium that precedes the vascular response.**

122 These observations raise the questions of how pyramidal neurons can induce
123 vasoconstriction at higher AP-firing rates. It is generally accepted that the synthesis and/or
124 release of vasodilatory substances requires an increase in intracellular Ca^{2+} in the releasing
125 cells[32,33], but little is known about the release of vasoconstricting substances. We therefore
126 determined whether an increase in somatic Ca^{2+} concentration in cortical neurons was also
127 dependent on photostimulation frequency. We combined optogenetic stimulation with
128 whole-cell current clamp recording and intracellular Ca^{2+} imaging using Rhod-2 delivered by
129 patch pipette (Fig. 2a). Excitation of this red Ca^{2+} indicator at 585 nm did not induce any
130 voltage response in the recorded pyramidal cells (Fig. 2a and supplementary Fig. 3), as
131 expected from the action spectrum of ChR2[27]. In contrast, photostimulation at 470 nm
132 elicited a train of spikes accompanied by a somatic Ca^{2+} increase that lasted tens of seconds
133 following photostimulation without triggering any significant recurrent spiking activity
134 (Supplementary Fig. 3). The Ca^{2+} response evoked by 20 Hz photostimulation was more than
135 twice of that evoked by 2 Hz photostimulation (Fig. 2b; 2 Hz: $\Delta F/F_0$= 34.5 ± 3.7 %, n= 9 cells,
136 vs. 20 Hz: $\Delta F/F_0$= 79.5 ± 17.7 %, n= 9 cells; $t_{(16)}$= 2.485, p= 0.024397), while the average
137 number of evoked spikes was about five times higher (Fig. 1a and supplementary Fig. 3).
138 These results demonstrate a frequency-dependent increase in intracellular Ca^{2+} induced by

139 photostimulation, that is temporally compatible with the synthesis and/or release of
140 vasoactive mediators and subsequent vasoconstriction. We therefore aimed to understand
141 the molecular mechanisms linking neuronal activity to vasoconstriction.

142 **Vasoconstriction induced by pyramidal cells requires spiking activity and is only partially**
143 **dependent on glutamatergic transmission.**

144 In pyramidal cells, APs induce both somatic Ca^{2+} elevation[34] and glutamate release. To
145 determine whether spiking activity is required for vasoconstriction induced by 20 Hz
146 photostimulation, we blocked APs with the voltage-activated sodium channel blocker
147 tetrodotoxin (TTX, 1 µM, n= 6 arterioles). This treatment completely abolished the
148 vasoconstriction evoked by 20 Hz photostimulation (Fig. 3; AUC= 0.4 ± 0.4 x 10^3 %.s, $t_{(14)}$=
149 5.57, p= 8.6656 x 10^{-6}). These data indicate that APs are mandatory for neurogenic response
150 and may involve glutamate release.

151 Indeed, high levels of glutamate released from pyramidal cells may activate vasoconstrictive
152 cells, including NPY-expressing interneurons or astrocytes, through activation of ionotropic
153 or group I metabotropic glutamate receptors[8,17,18]. It may also directly activate NMDA
154 receptors on arteriolar smooth muscle cells, resulting in a large intracellular Ca^{2+} increase
155 and subsequent vasoconstriction[15]. To test the hypothesis that glutamate from pyramidal
156 cells, either directly or indirectly, results in vasoconstriction, we blocked glutamatergic
157 transmission by antagonizing AMPA/kainate, NMDA and group I metabotropic receptors
158 expressed by cortical neurons[35,36] and juvenile astrocytes[37]. Glutamate receptor antagonists
159 reduced the magnitude of vasoconstriction (-1.6 ± 0.4 x 10^3 %.s, $t_{(18)}$= 3.28, p= 0.0160) by
160 approximately half (Fig. 3). Taken together, our data suggest that photostimulation of
161 pyramidal cells elicits a frequency-dependent vasoconstriction that requires their spiking
162 activity and partially involves glutamatergic transmission. We therefore sought to elucidate
163 the glutamate-independent vasoactive pathway underlying this neurogenic vascular
164 response.

165 **Pyramidal cells express the mRNAs for a cell autonomous PGE2 and PGF2α synthesis**

166 Several arachidonic acid metabolites produced after intracellular Ca^{2+} elevation, including
167 PGF2α, but also PGE2, exert dose-dependent vasoconstrictive effects[23,24,38]. These
168 prostaglandins could therefore be progressively released as the frequency of

169 photostimulation and somatic Ca^{2+} increase, and thereby promote vasoconstriction. Layer II-
170 III pyramidal cells have been shown to produce PGE2[22]. To determine whether the
171 synthesizing enzymes of PGE2 and PGF2α are present in pyramidal cells, we performed
172 single-cell RT-PCR after patch-clamp recording[39]. Sixteen layer II-III pyramidal cells were
173 visually identified based on the triangular shape of their soma and a prominent apical
174 dendrite. Their glutamatergic phenotype was confirmed both by their stereotypical regular
175 spiking firing pattern (Fig. 4a) and also by the expression of the vesicular glutamate
176 transporter, vGlut1, and neither of the two GABA synthesizing enzymes (Fig. 4b)[28]. The rate-
177 limiting enzymes of prostaglandin synthesis, cyclooxygenase-1 (COX-1) and -2 (COX-2), were
178 detected in 25% (n= 4 of 16 cells) and 31% (n= 5 of 16 cells) of pyramidal cells, respectively,
179 (Fig. 4b-d) but were never co-expressed (Fig. 4d). The cytosolic enzyme responsible for
180 synthesizing PGE2 (cPGES) was observed in most pyramidal cells (Fig. 4b-c; 88%, n= 14 of 16
181 cells). In addition, the microsomal PGES, mPGES1 and mPGES2 were detected in 6% (Fig. 4c,
182 n= 1 of 16 cells) and 38% (Fig. 4b,c; n= 6 of 16 cells) of pyramidal cells, respectively, and were
183 always co-expressed with cPGES. The PGF2α terminal-synthesizing enzyme AKR1B3 was
184 observed in the majority of neurons (Fig. 4b-c; n= 11 of 16 cells, 69%). Occasionally, it was
185 co-detected with the prostamide/prostaglandin F synthase (PM-PGFS, Fig. 4c, n= 5 of 16
186 cells, 31%) and the PGE2 converting enzyme carbonyl reductase 1 (CBR1, Fig. 4c; n= 3 of 16
187 cells, 19%). CBR1 was consistently detected alongside at least one PGES. Pyramidal cells
188 positive for COX-1 also expressed PGES (Fig. 4d), with most of them also co-expressing PGFS
189 (n=3 out of 4). All neurons positive for COX-2 co-expressed both PGES and PGFS (Fig. 4d).
190 These molecular observations suggest that subpopulations of layer II-III pyramidal cells
191 express all the necessary transcripts for the synthesis of PGE2 and PGF2α .

192 **Prostaglandins underpin vasoconstriction *ex vivo* and *in vivo*.**

193 To investigate whether prostaglandins could mediate neurogenic vasoconstriction, we
194 inhibited their synthesis. The non-selective COX inhibitor indomethacin (5 µM,
195 supplementary Table 3, Fig. 5a) completely abolished the vascular response (n= 10
196 arterioles, AUC= 0.0 ± 0.2 x 10^3 %.s, $t_{(18)}$= 5.86, p= 3.4385 x 10^{-5}). *In vivo* monitoring of pial
197 artery diameter changes by 2-photon imaging (Fig. 5c and d) during 10 Hz photostimulation
198 of anesthetized Emx1-cre;Ai32 mice revealed that pyramidal cells induce vasodilation
199 followed by sustained vasoconstriction (Fig. 5d and e). This confirms and expands upon

200 previous *in vivo* observations[8]. The constriction phase was inhibited by indomethacin (i.v.),
201 indicating the involvement of prostaglandins in the vasoconstriction (AUC_{Ctrl}= -291.5 ± 92.4
202 %.s vs. $AUC_{Indo.}$= 332.4 ± 184.4 %.s, $U_{(5,4)}$= 0, p= 0.0159, Fig. 5d-f), which confirms our *ex vivo*
203 observations. To determine whether they originated from COX-1 or COX-2 activity, we
204 utilized selective inhibitors. The vasoconstriction magnitude was reduced by the COX-1
205 inhibitor SC-560 (100 nM, n= 10 arterioles, supplementary Table 3) (-1.4 ± 0.7 x 10^3 %.s, $t_{(18)}$=
206 3.54, p= 9.3396 x 10^{-3}, Fig. 5b-c). The COX-2 inhibitor NS-398 (10 µM, n= 7 arterioles,
207 supplementary Table 3) completely abolished pyramidal cell-induced vasoconstriction in a
208 more potent manner (Fig. 5b; AUC= 0.1 ± 0.3 x 10^3 %.s, $t_{(15)}$= 5.45, p= 1.0853 x 10^{-5}). These
209 observations suggest that prostaglandins, derived mainly from COX-2 activity, and to a lesser
210 extent from COX-1 activity, mediate pyramidal cell-induced vasoconstriction.

211 **PGE2 mediates vasoconstriction by acting primarily on EP1 receptor.**

212 To determine the nature of the prostaglandins and their receptors, we selectively
213 antagonized the vasoconstrictor receptors of PGE2, EP1 or EP3, or the FP receptor of PGF2α.
214 The magnitude of vasoconstriction was reduced by the selective EP1 receptor antagonist
215 ONO-8130 (10 nM, n= 9 arterioles, Fig. 6, 0.3 ± 0.3 x 10^3 %.s, $t_{(17)}$= 6.01, p= 2.8451 x 10^{-6},
216 supplementary Table 3), and to a lesser extent, by the EP3 receptor antagonist L-798,106 (1
217 µM, n= 9 arterioles, Fig. 6, -0.9 ± 0.4 x 10^3 %.s, $t_{(17)}$= 4.30, p= 8.0261 x 10^{-4}, supplementary
218 Table 3). Impairing FP receptor signaling with AL-8810 (10 µM, n= 9 arterioles, Fig. 6,
219 Supplementary table 3) tended to reduce the evoked vasoconstriction, however, it did not
220 reach statistical significance (AUC= -1.9 ± 0.4 x 10^3 %.s, $t_{(17)}$= 2.82, p= 0.0533). Additionally,
221 the pre-constricted state induced by this weak partial FP agonist[40] (supplementary Fig. 6f)
222 resulted in a diameter reduction of approximately 4% (diameter before application 21.8 ±
223 2.5 µm vs. during 20.9 ± 2.6 µm, n= 9 arterioles, $t_{(8)}$= 2.374, p= 0.0457, paired t-test), which
224 underestimated the optogenetic vascular response. Taken together, these results indicate
225 that pyramidal cell photoactivation induces vasoconstriction through the release of PGE2
226 originating from COX-2. This effect primarily acts on the EP1 receptor and, to a lesser extent,
227 on the EP3 receptor.

228 To test a direct effect of PGE2 through vascular EP1/EP3 activation, we determined whether
229 exogenous agonists of PGE2 receptors could mimic the vasoconstriction induced by
230 pyramidal cell photostimulation. Similar to increasing photostimulation frequencies,

231 exogenous application of PGE2 induced vasoconstriction in a dose dependent manner
232 (Supplementary Fig. 7a). Likewise, 10 µM sulprostone, an EP1/EP3 agonist with an EC_{50}
233 comparable to that of PGE2[41], mimicked the vasoconstriction induced by 1-10 µM PGE2
234 (Supplementary Fig. 7b). Application of 10 µM PGE2 in the presence of TTX did not impair
235 the evoked vasoconstriction (Supplementary Fig. 7c). These observations suggest that PGE2
236 and its EP1 and EP3 receptors mediate the neurogenic vasoconstriction and that once PGE2
237 is released, its vascular effect is independent of spiking activity.

238 **Astrocytes through 20-HETE and NPY interneurons are indirect intermediates of pyramidal**
239 **cell-induced vasoconstriction.**

240 In addition to smooth muscle cells, PGE2 released by pyramidal cells can also activate
241 astrocytes and neurons[42,43], which also express its receptors[35,36]. To assess whether
242 astrocytes could mediate the PGE2-dependent vasoconstriction, we first targeted the large
243 conductance Ca^{2+}-activated (BK) channels and the 20-HETE pathways, both of which mediate
244 astrocyte-derived vasoconstriction dependent on glutamatergic transmission[17,18]. Blockade
245 of BK channels with paxilline (1 µM, n= 10 arterioles, Supplementary table 3) did not impair
246 the vascular response (Fig. 7; AUC = $-3.7 \pm 0.3 \times 10^3$ %.s, $t_{(18)} = 0.03$, $p = 1$). Selective
247 inhibition of the 20-HETE synthesizing enzyme, CYP450 ω-hydroxylase, with HET-0016 (100
248 nM, n= 10 arterioles, Supplementary table 3) reduced the magnitude of the evoked
249 vasoconstriction (Fig. 7; AUC = $-1.6 \pm 0.7 \times 10^3$ %.s, $t_{(18)} = 3.32$, $p = 0.0160$). These data
250 suggest that astrocytes partially mediate the vasoconstriction induced by pyramidal cells via
251 20-HETE but not via K^+ release. We next determined whether NPY, a potent
252 vasoconstrictor[16], was involved in neurogenic vasoconstriction. Antagonism of the NPY Y1
253 receptors by BIBP3226 (1 µM, n= 10 arterioles, Supplementary table 3) completely abolished
254 neurogenic vasoconstriction (Fig. 6; AUC = $-0.3 \pm 0.2 \times 10^3$ %.s, $t_{(18)} = 5.28$, $p = 1.9512 \times 10^{-5}$).
255 These results suggest that neurogenic vasoconstriction induced by pyramidal cells
256 photostimulation involves the activation of NPY-expressing interneurons and Y1
257 receptors[8,16,28] and astrocytes via 20-HETE in glutamatergic-dependent and -independent
258 manners.

Discussion

This study establishes that pyramidal cells activity leads to arteriole vasoconstriction, and the magnitude of the vasoconstriction depends on AP firing frequency and correlates with a graded increase in pyramidal cell somatic Ca^{2+}. This vascular response requires AP firing and partially involves glutamatergic transmission through direct and indirect mechanisms on arteriolar smooth muscle cells. *Ex vivo* and *in vivo* observations revealed that PGE2, predominantly produced by layer II-III COX-2 pyramidal cells, and its EP1 and EP3 receptors play a crucial role in neurogenic vasoconstriction. Pharmacological evidence indicates that some interneurons, via NPY release and activation of Y1 receptors, and to a lesser extent, astrocytes through 20-HETE and possibly COX-1 derived PGE2 play an intermediary role in this process (Figure 8).

We found that increasing the frequency of photostimulation in an ex vivo preparation caused nearby arteriole to go from a barely discernible response to robust vasoconstriction. In contrast, *in vivo* observations have shown that the optogenetic stimulation of pyramidal cells induces a hyperemic/vasodilatory response[22,44,45], that can be followed by vasoconstriction[8]. This biphasic response was confirmed *in vivo.* However, a more pronounced vasoconstriction phase was observed when using high frequency 10-second-long periods of photostimulation (Fig. 5). The difficulty in observing vasodilation in cortical slices may be due to relaxed arterioles which favor vasoconstriction[46]. However, the evidence that neurogenic vasoconstriction is frequency-dependent (Fig. 1) and that pharmacologically-induced vasoconstriction persists in preconstricted[18] or pressurized arterioles[24], suggests that the neurogenic vasoconstriction primarily depends on a high pyramidal cell firing rate rather than on vascular tone. The mandatory role of action potentials indicates that Ca^{2+} entry via ChR2 alone is insufficient to drive a vascular response. This likely reflects the essential role of voltage-gated Ca^{2+} channels in somatic Ca^{2+} elevation[47] and the subsequent release of neuronal vasoactive agents[8,22].

Most previous observations did not report a decreased in CBF induced by optogenetic stimulation of pyramidal cells *in vivo*[22,45]. This may be attributed to differences in the photostimulation paradigm and/or the specific subtype of pyramidal cells that were stimulated. In our study, we used 10 seconds of photostimulation both *in vivo* and *ex vivo*. Earlier studies have employed shorter photostimulation times, lasting no more than 1

290 second[8,22,45], which may have resulted in an insufficient number of elicited APs to induce
291 robust vasoconstriction. Furthermore, we observed that neurogenic vasoconstriction is
292 highly dependent on COX-2, which is primarily expressed in layer II-III pyramidal cells[22,35,36].
293 In our study, photostimulation of almost all pyramidal cells in Emx1-Cre;Ai32 mice[25,26] likely
294 resulted in the release of more COX-2 metabolites. Thy1-ChR2 mice used in previous
295 studies[8,45], on the other hand, express primarily ChR2 in layer V pyramidal cells[44,] which
296 rarely express COX-2.

297 Our *ex vivo* and *in vivo* observations revealed that PGE2, primarily derived from COX-2, plays
298 a critical role in neurogenic vasoconstriction by activating EP1 and EP3 receptors expressed
299 by vascular smooth muscle cells[15]. Previous studies have shown that COX-2 pyramidal cells,
300 when activated *in vivo* by sensory stimulation or *ex vivo*, induce a NMDA-dependent increase
301 in CBF and vasodilation through PGE2 and EP2/EP4 receptors[19,22,48]. Differences in the levels
302 and/or sites of action of released PGE2 may explain the absence of secondary
303 vasoconstriction. In Emx1-Cre;Ai32 mice[25,26], optogenetic stimulation may have activated a
304 greater number of COX-2 pyramidal cells and resulted in a higher local release of PGE2
305 compared to sensory stimulation. A high level of PGE2 may have facilitated the activation of
306 the EP1 receptor, which has a lower affinity than the EP2/EP4 receptors[41]. Additionally, it
307 may have promoted the rapid desensitization of the dilatory EP4 receptor[49] thereby favoring
308 vasoconstriction. Furthermore, PGE2 can induce either EP1-dependent arteriolar dilation or
309 constriction depending on whether it is locally applied to capillaries or arterioles.
310 Constriction prevails when both segments are exposed[23]. Our photostimulation focused on
311 superficial penetrating arterioles, which lack a capillary network in their close vicinity[50]. This
312 may have facilitated the direct EP1-mediated arteriolar constriction[23,24]. Overall, these
313 observations suggest that COX-2 pyramidal cells can sequentially promote both vasodilation
314 and vasoconstriction through the release of PGE2, depending on the context.

315 Consistent with previous reports in rodents[22,35,36,51], the transcripts of the rate-limiting
316 enzymes COX-1 and COX-2, were detected in subpopulations of mouse layer II-III pyramidal
317 cells, respectively. COX-1/2 expression was found to be systematically associated with at
318 least one PGE2 synthesizing enzyme. The major isoforms were cPGES and mPGES2, with the
319 latter being less prevalent[22,35,36]. The low detection rate of mPGES1, an isoform co-induced
320 with COX-2 by various stimuli[52,53], reflects its low constitutive basal expression level. The

321 presence of PM-PGFS, CBR1 and AKR1B3 in layer II-III pyramidal cells is consistent with
322 single-cell RNAseq data[35,36]. The expression of a PGFS was systematically observed in COX-2
323 positive pyramidal cells and in a majority of COX-1 positive neurons, similar to PGES. These
324 observations collectively indicate that subpopulations of layer II-III pyramidal cells express
325 the mRNAs required for PGE2 and PGF2α synthesis derived from COX-1 or COX-2 activity.
326 Our pharmacological observations did not reveal a contribution of PGF2α in neurogenic
327 vasoconstriction, despite the potential ability of pyramidal cells to produce it. This is likely
328 because PGF2α is only detectable in pyramidal neurons under conditions where COX-2 is
329 over-expressed[54].

330 Pyramidal cells may have an indirect effect on vascular activity through the activation of
331 intermediate cell types, in addition to the direct vascular effects of PGE2 and glutamate[15.]
332 Consistent with previous observations, we found that glutamate transmission from
333 pyramidal cells is involved to some extent[8]. Additionally, we found that the NPY Y1 receptor
334 plays a key role in neurogenic vasoconstriction. It is likely that glutamatergic transmission
335 contributed to NPY release, considering that NPY GABAergic interneurons express a wide
336 range of ionotropic and metabotropic glutamate receptors[35,36]. Consistently, the Y1 receptor
337 has been shown to be involved in vasoconstriction induced by sensory and optogenetic
338 stimulation of GABAergic interneurons[8]. This vascular response originates in deep layers and
339 propagates upstream to the pial surface. The density of neuronal-arteriolar smooth muscle
340 cell junctions[15] and of NPY interneurons[35] is higher in deep layers, supporting an initial
341 activation in those layers. However, layer I contains numerous NPY interneurons[28,35] and
342 exhibits strong Y1 receptor immunoreactivity in smooth muscle cells[55]. This suggests that
343 neurogenic vasoconstriction may also be relayed by superficial NPY interneurons.

344 Activation of group I metabotropic receptors in perivascular astrocytes has been shown to
345 promote vasoconstriction via BK channel-dependent K^+ release[18] or 20-HETE[17]. However, the
346 neurogenic vasoconstriction was not affected by the blockade of BK channels, which rules
347 out this astrocytic pathway. In contrast, the inhibition of ω-hydroxylase partially reduced
348 neurogenic vasoconstriction, suggesting the involvement of 20-HETE. Additionally,
349 astrocytes may also have contributed to vasoconstriction through the release of PGE2
350 derived from COX-1[56], as indicated by its mild impairment under SC-560. Pyramidal cells may
351 have indirectly contributed to neurogenic vasoconstriction via the release of PGE2, in

352 addition to glutamate. Indeed, GABAergic interneurons and astrocytes express PGE2
353 receptors[35,36], and PGE2 has been shown to induce neuronal firing and increase Ca^{2+} levels in
354 astrocytes[42,43]. Therefore, glutamate and PGE2 released from pyramidal cells may act
355 synergistically to indirectly promote vasoconstriction.

356 Although the vasoconstriction observed in epilepsy[9], shares similar mechanisms with the
357 neurogenic vasoconstriction described here, it differs in several aspects. Epileptic seizures
358 induce long-lasting hypoperfusion leading to severe hypoxia and memory and cognitive
359 impairment[9]. The high level of glutamate associated with epilepsy is likely to contribute to
360 the direct contraction of smooth muscle cell[15]. Like neurogenic vasoconstriction, seizure-
361 induced hypoperfusion is dependent on COX-2[9,10] and, to some extent on PGE2[9], likely
362 through EP1 and/or EP3 receptors. However, epileptic seizures induce the overexpression of
363 both COX-2 and mPGES1[51,53]. Additionally, PGF2α synthesis by COX-2 pyramidal cells is also
364 produced during seizures[54], suggesting that PGF2α and the FP receptors may also be
365 involved in this hypoperfusion.

366

367 Here, using multidisciplinary approaches, we describe a new mechanism of vasoconstriction
368 that depends on a high firing rate of pyramidal cells. This neurogenic vasoconstriction
369 primarily involves the release of COX-2-derived PGE2 and activation of EP1 and EP3
370 receptors. It is mediated by direct effects on vascular smooth muscle cells but also by
371 indirect mechanisms involving NPY release from GABAergic interneurons and astrocytes by
372 20-HETE synthesis. In contrast to previously described mechanisms of neurogenic
373 vasoconstriction, that have been mostly associated with GABAergic interneurons and
374 neuronal inhibition[3,8,16,57,58], our data suggest the involvement of glutamatergic excitatory
375 neurons and increased neuronal activity. This finding will help to update the interpretation
376 of the functional brain imaging signals used to map network activity in health and disease[2,59].
377 This excitatory form of neurogenic vasoconstriction may also help to understand the
378 etiopathogenesis of epilepsy[9,10] and Alzheimer's disease[60] in which increased cortical
379 network activity and hypoperfusion often overlap.

380 **Methods**

381 **Animals**

382 Homozygous Emx1-Cre mice [Jackson Laboratory, stock #005628, B6.129S2-Emx1$^{tm1(cre)Krj}$/J
383 [25]] were crossed with homozygous Ai32 mice [Jackson Laboratory, stock #012569, B6;129S-
384 Gt(ROSA)26Sor$^{tm32(CAG-COP4*H134R/EYFP)Hze}$/J [26]] to obtain heterozygous Emx1$^{cre/WT}$;Ai32$^{ChR2/WT}$
385 mice for optogenetic stimulations. C57BL/6RJ mice were used for PGE2 and sulprostone
386 exogenous applications, control optogenetic experiments and single-cell RT-PCR. 16-21
387 postnatal day-old females and males were used for all *ex vivo* experiments. Female
388 Emx1$^{cre/WT}$;Ai32$^{ChR2/WT}$ mice, 3 to 5-month-old, were used for *in vivo* experiments.

389 All experimental procedures using animals were carried out in strict accordance with French
390 regulations (Code Rural R214/87 to R214/130) and conformed to the ethical guidelines of
391 the European Communities Council Directive of September 22, 2010 (2010/63/UE). Mice
392 were fed *ad libitum* and housed in a 12-hour light/dark cycle. *In vivo* experiments were done
393 in accordance with the Institut national de la santé et de la recherche médicale (Inserm)
394 animal care and approved by the ethical committee Charles Darwin (Comité national de
395 réflexion éthique sur l'expérimentation animale – n°5) (protocol number #27135
396 2020091012114621).

397 ***Ex vivo* slice preparation**

398 Mice were deeply anesthetized by isoflurane (IsoVet, Piramal Healthcare UK or IsoFlo,
399 Axience) evaporation in an induction box then euthanized by decapitation. The brain was
400 quickly removed and placed in cold (~4°C), oxygenated artificial cerebrospinal fluid (aCSF)
401 containing (in mM): 125 NaCl, 2.5 KCl, 1.25 NaH2PO4, 2 CaCl2, 1 MgCl2, 26 NaHCO3, 10
402 glucose, 15 sucrose and 1 kynurenic acid (Sigma-Aldrich). 300 µm-thick coronal slices
403 containing the barrel cortex were cut with a vibratome (VT1000s; Leica) and were allowed to
404 recover at room temperature for at least 45 min with oxygenated aCSF (95% O2/5% CO2)[39].
405 The slices were then transferred to a submerged recording chamber and continuously
406 perfused at a rate of 2 ml/min with oxygenated aCSF lacking kynurenic acid.

407 **Whole-cell recordings**

408 Patch pipettes (5.5 ± 0.2 MΩ) pulled from borosilicate glass were filled with 8 µl of RNase
409 free internal solution containing (in mM): 144 K-gluconate, 3 MgCl2, 0.5 EGTA, 10 HEPES, pH

410 7.2 (285/295 mOsm). For electrophysiological recordings combined with calcium imaging,
411 EGTA was replaced by 200 µM Rhod-2 (20777, Cayman chemicals). Whole-cell recordings
412 were performed at room temperature (20-25 °C) using a patch-clamp amplifier (Axopatch
413 200B, MDS). Data were filtered at 5-10 kHz and digitized at 50 kHz using an acquisition board
414 (Digidata 1440, MDS) attached to a personal computer running pCLAMP 10.2 software
415 package (MDS). Electrophysiological properties were determined in current-clamp mode[28].
416 Membrane potential values were corrected for theoretical liquid junction potential (−15.6
417 mV). Resting membrane potential of neurons was measured immediately after passing in
418 whole-cell configuration. Only neurons with a resting membrane potential more
419 hyperpolarized than −60 mV were analyzed further.

420 **Optogenetic stimulation**

421 Optogenetic stimulation was achieved through the objective using a 470 nm light emitting
422 device (LED, CoolLED, Precise Excite) attached to the epifluorescence port of a BX51WI
423 microscope (Olympus) and a set of multiband filters consisting of an excitation filter (HC
424 392/474/554/635, Semrock), a dichroic mirror (BS 409/493/573/652, Semrock), and an
425 emission filter (HC 432/515/595/730, Semrock). Photostimulation consisted of a 10-s train of
426 5 ms light pulses at an intensity of 38 mW/mm² and delivered at five different frequencies
427 (1, 2, 5, 10 and 20 Hz).

428 **Infrared imaging**

429 Blood vessels and cells were observed in slices under infrared illumination with Dodt
430 gradient contrast optics (IR-DGC, Luigs and Neumann) using a double-port upright
431 microscope (BX51WI, Olympus) and a collimated light emitting device (LED; 780 nm;
432 ThorLabs) as the transmitted light source, a 40X (LUMPlanF/IR, 40X/0.80 W, Olympus) or a
433 60X (LUMPlan FL/IR 60X/0.90 W, Olympus) objective and a digital camera (OrcaFlash 4.0,
434 Hamamatsu) attached to the front port of the microscope. Penetrating arterioles in layer I
435 were selected by IR-DGC videomicroscopy based on their well-defined luminal diameter (10-
436 40 µm), their length remaining in the focal plane for at least 50 µm[22], and the thickness of
437 their wall (4.1 ± 0.1 µm, n = 176 blood vessels). A resting period of at least 30 min[38] was
438 observed after slice transfer. After light-induced responses, arteriolar contractility was
439 tested by the application of aCSF containing the thromboxane A2 agonist, U46619 (100
440 nM)[16] or K^+ enriched solution (composition in mM: 77.5 NaCl, 50 KCl, 1.25 NaH2PO4, 2 CaCl2,

441 1 MgCl2, 26 NaHCO3, 10 glucose, 15 sucrose). Vessels that did not constrict with these
442 applications were discarded. Only one arteriole was monitored per slice. IR-DGC images
443 were acquired at 0.1 Hz for pharmacological applications and at 1 Hz for optogenetic
444 experiments using Imaging Workbench 6.1 software (Indec Biosystems). The focal plane was
445 continuously maintained on-line using IR-DGC images of cells as anatomical landmarks[22].

446 **Calcium imaging**

447 Visually and electrophysiologically identified layer II-III pyramidal cells were filled with the
448 calcium-sensitive dye Rhod-2 (200 µM, Cayman chemicals, 20777) using patch pipettes.
449 Optical recordings were made at least 15 min after passing in whole-cell configuration to
450 allow for somatic diffusion of the dye. Rhod-2 was excited with a 585 nm LED (Cool LED,
451 Precise Excite) at an intensity of 0.56 mW/mm² and the filter set used for optogenetic
452 stimulation using the Imaging Workbench 6.1 software (Indec Byosystems). IR-DGC and
453 fluorescence images were acquired by alternating epifluorescence and transmitted light
454 sources. IR-DGC and fluorescence were respectively sampled at 5 Hz and 1 Hz during
455 baseline and optogenetic stimulation, respectively, and at 1 Hz and 0.2 Hz after
456 photostimulation. During photostimulation, bleed-through occurred in the Rhod-2 channel
457 due to the fluorescence of the EYFP-ChR2 transgene[26]. Therefore, the Ca^{2+} response could
458 not be reliably analyzed during this period. To compensate for potential x-y drifts, all images
459 were registered off-line using the "StackReg" plug-in[61] of the ImageJ 1.53 software. To define
460 somatic regions of interest (ROIs), the soma was manually delineated from IR-DGC images.
461 Fluorescence intensity changes ($\Delta F/F_0$) were expressed as the ratio $(F-F_0)/F_0$ where F is the
462 mean fluorescence intensity in the ROI at a given time point, and F_0 is the mean fluorescence
463 intensity in the same ROI during the 30-s control baseline.

464 **Drugs**

465 All pharmacological compounds were bath applied after a 5-min baseline, and vascular
466 dynamics were recorded during bath application. The following drugs were dissolved in
467 water: D-(-)-2-amino-5-phosphonopentanoic acid (D-AP5, 50 µM, Hellobio, HB0225), 6,7-
468 dinitroquinoxaline-2,3-dione (DNQX, 10µM, Hellobio, HB0262), LY367385 (100µM, Hellobio,
469 HB0398) and BIBP3226 (1 µM, Tocris, 2707). Tetrodotoxin (TTX, 1 µM, L8503, Latoxan) was
470 dissolved in 90 % acetic acid. PGE2 (HB3460, Hellobio), sulprostone (10 µM, Cayman
471 chemical, 14765), 2-methyl-6-(phenylethynyl)pyridine (MPEP, 50 µM, Hellobio, HB0426) and

472 9,11-dideoxy-9α,11α-methanoepoxy prostaglandin F2α (U-46619, 100 nM, Enzo, BML-
473 PG023) were dissolved in ethanol. Indomethacin (5 µM, Sigma-Aldrich, I7378), SC-560 (100
474 nM, Sigma-Aldrich, S2064-5MG), NS-398 (10 µM, Enzo, BML-EI261), ONO-8130 (10 nM,
475 Tocris, 5406), L-798,106 (1 µM, Cayman chemical, 11129), AL8810 (10 µM, Cayman chemical,
476 16735), paxilline (10 µM, Tocris, 2006) and HET0016 (100 µM, Merck, SML2416-5MG) in
477 DMSO. Acetic acid, ethanol and DMSO doses were always used below 0.1%. Synthesis
478 inhibitors and BIBP3226 were applied at least 30 minutes before optogenetic stimulation.
479 TTX was applied at least 15 minutes before, while glutamate receptor antagonists and
480 paxilline were applied at least 10 and 5 minutes before, respectively.

481 **Vascular reactivity analysis**

482 To compensate for potential x-y drifts, all images were realigned off-line using the
483 "StackReg" plug-in[61] of the ImageJ 1.53 software. Luminal diameter was measured in layer I
484 on registered images using custom analysis software developed in MATLAB (MathWorks)[22].
485 To avoid potential drawbacks due to vessel instability, only arterioles with a stable diameter
486 were analyzed further. Arterioles were considered stable if the relative standard deviation of
487 their diameter during the baseline period was less than 5%[22]. Comparison of the mean
488 arteriolar diameter during the 5-minute baseline and the 5-minute final pharmacological
489 treatments revealed that all drugs, except AL8810, had no effect on resting diameter
490 (Supplementary Fig. 4, 6 and 8).

491 Diameter changes ($\Delta D/D_0$) were expressed as $(D_t - D_0)/D_0$ where D_t is the diameter at the
492 time t and D_0 is the mean diameter during the baseline period. To eliminate sharp artifacts
493 due to transient loss of focus, diameter change traces were smoothed using a sliding three-
494 point median filter. The overall vascular response over time was captured by the area under
495 the curve of diameter changes after photostimulation. Graphs were generated using R
496 software version 4.3.0[62] and Matplotlib package[63].

497 **Intrinsic optical signals analysis**

498 Variations in IR light transmittance (ΔT)[30] were determined using ImageJ 1.53 software
499 according to: $\Delta T = (T_t - T_0)/ T_0$ where T_t is the light transmittance at a time t and T0 is the
500 average light transmittance during the baseline period of a squared region of interest of 100
501 µm x 100 µm manually delineated in layer I. The rate of ΔT change was determined as the
502 first derivative of ΔT ($d\Delta T/dt$, where ΔT is the change in light transmittance and t is time).

503 Slices that showed a maximum rate of increase of dΔT/dt greater than 2%/s, indicating the
504 occurrence of spreading depression[30], were excluded.

505 **Surgery**

506 Chronic cranial windows were implanted one week after the head bar surgery as previously
507 described[64]. We used a 100 µm thick glass coverslip over the barrel cortex (~3mm^2). Before
508 two-photon experiments, a recovery period of 7-10 days minimum was maintained.

509 **Two-photon imaging and photostimulation**

510 For two-photon excitation, we used a femtosecond laser (Mai Tai eHP; SpectraPhysics) with
511 a dispersion compensation module (Deepsee; SpectraPhysics) emitting 70-fs pulses at 80
512 MHz. The laser power was attenuated by an acousto-optical modulator (AA Optoelectronic,
513 MT110-B50-A1.5-IR-Hk). Scanning was performed with Galvanometric scanner (GS) mirrors
514 (8315KM60B; Cambridge Technology). Fluorescein was excited at 920 nm and the emitted
515 light was collected with a LUMFLN60XW (Olympus, 1.1 NA) water immersion objective.
516 Collected photons were sorted using a dichroic mirror centered at 570 nm, a FF01-525/25
517 nm filter (Semrock) and a GaAsP (Hamamatsu) photomultipliers tube. Customized LabView
518 software was used to control the system. Line-scan were drawn across pial vessels to
519 measure diameter change.

520 Mice were anesthetized with a mixture of ketamine and medetomidine (100 and 0.5 mg⁄kg,
521 respectively, intraperitoneal (i.p.)) during imaging sessions. Body temperature was
522 maintained at 36.5°C using a retro-controlled heating pad. Fluorescein dextran (70 kDa) was
523 injected i.v. through a retro-orbital injection to label brain vessels. Mice received continuous
524 air through a nose cone supplemented with oxygen to reach a final concentration of 30% O_2.
525 Photostimulation was delivered with a 473 nm laser (Coblot MLD, Sweden) through an optic
526 fiber placed above the glass coverslip and directed at the pial artery of interest. Each
527 photostimulation consisted of a 10-s train of 5 ms light pulses delivered at 10 Hz, respecting
528 a 5 minutes interstimulus interval. Indomethacin (10mg/kg, #15425529, Thermo Fisher
529 Scientific) was administered i.v. through a retroorbital injection.

530 **Imaging analysis**

531 Pial arteriole diameter change was determined with line-scan acquisitions and a home-made
532 Matlab script as previously described[11]. Trials from the same vessel were averaged (with a

533 0.1 s interpolation) for analysis. Area under the curve and statistics were performed using
534 GraphPad Prim (version 6).

535 **Cytoplasm harvesting and single-cell RT-PCR**

536 At the end of the whole-cell recording, which lasted less than 15 min, the cytoplasmic
537 content was collected in the recording pipette by applying a gentle negative pressure. The
538 pipette's content was expelled into a test tube and RT was performed in a final volume of 10
539 µl as described previously[39]. The scRT-PCR protocol was designed to probed simultaneously
540 the expression of prostaglandins synthesizing enzymes and neuronal markers[22].
541 Prostaglandins synthesizing enzymes included COX-1 and COX-2, the terminal PGE2
542 synthases (PGES): mPGES1, mPGES2 and cPGES, the terminal PGF2α synthases (PGFS): PM-
543 PGFS (Prxl2b) and AKR1B3 and the carbonyl reductase CBR1. Neuronal markers included the
544 vesicular glutamate transporter, vGluT1, and the two isoforms of glutamic acid
545 decarboxylase, GAD65 and GAD67. Two-step amplification was performed essentially as
546 described[39]. First, cDNAs present in the 10 µl reverse transcription reaction were
547 simultaneously amplified with all external primer pairs listed in Supplementary table 2. Taq
548 polymerase (2.5 U; Qiagen) and external primers mix (20 pmol each) were added to the
549 manufacturer's buffer (final volume, 100 µl), and 20 cycles (95◦C, 30 s; 60◦C, 30 s; and 72◦C,
550 35 s) of PCR were performed. Second rounds of PCR were performed using 1 µl of the first
551 PCR product as a template. In this second round, each cDNA was amplified individually using
552 its specific nested primer pair (Supplementary table 2) by performing 35 PCR cycles (as
553 described above). 10 µl of each individual PCR product were run on a 2% agarose gel stained
554 with ethidium bromide using ΦX174 digested by *HaeIII* as a molecular weight marker. The
555 efficiency of the protocol was validated using 500 pg of total forebrain RNAs (Supplementary
556 Fig. 5).

557 **Statistical analyses**

558 Statistical analyses were performed using GraphPad Prism version 7.00 for Windows
559 (GraphPad Software, La Jolla California USA, www.graphpad.com) and R software version
560 4.3.0[62]. Normality of distribution was assessed using the Shapiro-Wilk tests. Equality of
561 variance was assessed using Brown-Forsythe tests for comparisons between groups and
562 using F-tests for comparisons with a control group. Parametric tests were only used if these
563 criteria were met. Statistical significance of morphological and physiological properties of

564 penetrating arterioles was determined using one-way ANOVA for comparison between
565 groups. Statistical significance of calcium was determined using two-tailed unpaired t-tests
566 and Statistical significance of vascular responses were appreciated using Tukey posthoc tests
567 for the different frequencies conditions and using Dunnett's posthoc tests for the different
568 pharmacological conditions compared to the 20 Hz condition without pharmacological
569 compound. False discovery rate correction was used for multiple comparisons. Statistical
570 significance of vascular diameter for drug applications was determined using two-tailed
571 paired t-tests. Statistical significance on all figures uses the following convention: *$p<0.05$,
572 **$p<0.01$ and ***$p<0.001$.

573 **Data availability statement**

574 The data that support the results of this study are available from the corresponding author
575 upon reasonable request.

576 **Acknowledgements**

577 The authors thank Dr Rebecca Piskorowski for constructive criticism of the manuscript. We
578 acknowledge the invaluable support of the animal facilities of IBPS (RongIBPS) and Institut
579 de la vision for their expert care and maintenance of the animals used in this study. Financial
580 support was provided by grants from the Agence Nationale pour la Recherche (ANR-17-
581 CE37-0010-03, B.C.; CE37_2020_TF-fUS-CADASIL, S.C.; ANR-20-CE14-0025, D.L.; ANR-23-
582 CE14-0038-01, B.C.), the Fondation Alzheimer France (M21JRCN009, S.C.) and the i-Bio
583 initiative of Sorbonne University (B.C.). B.L.G. and E.B. were supported by fellowships from
584 Fondation pour la Recherche sur Alzheimer and M.T. by a fellowship from the Fondation
585 pour la Recherche Médicale (SPF201909009103).

586 **Author contributions**

587 B.L.G., M.T., and E.B. designed experiments, acquired, and analyzed the data, and edited the
588 manuscript. S.P. acquired the data. B.L.G. and B.C. drafted the manuscript. I.D. edited the
589 manuscript. H.S. analyzed the data. D.L. designed experiments and edited the manuscript.
590 S.C. and B.C. designed experiments and edited the manuscript.

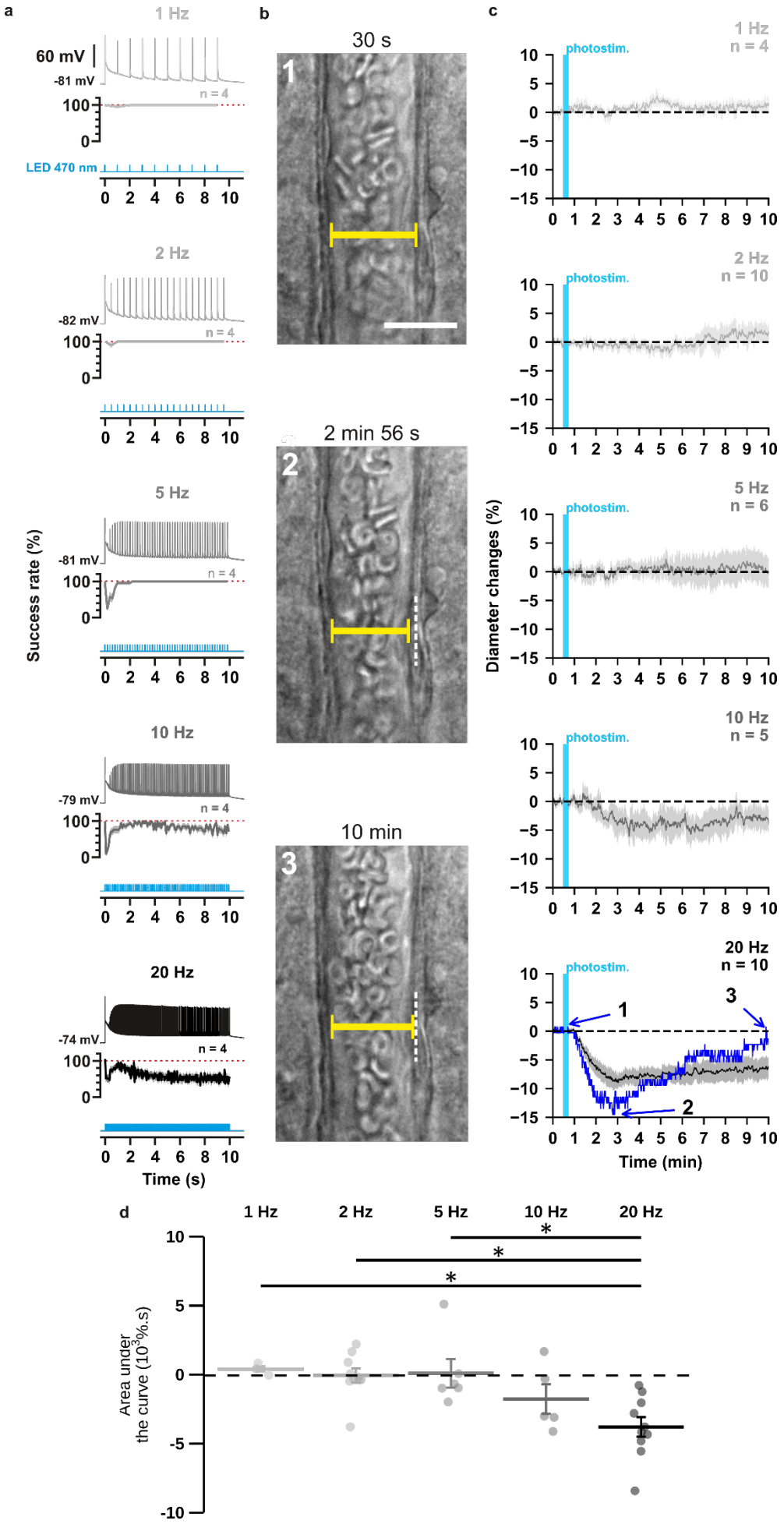
a
1 Hz
60 mV
-81 mV
n = 4
100
0
LED 470 nm
0 2 4 6 8 10
2 Hz
-82 mV
n = 4
5 Hz
-81 mV
n = 4
10 Hz
-79 mV
n = 4
20 Hz
-74 mV
n = 4
Success rate (%)
Time (s)
b
30 s
1
2 min 56 s
2
10 min
3
c
1 Hz
n = 4
photostim.
2 Hz
n = 10
5 Hz
n = 6
10 Hz
n = 5
20 Hz
n = 10
Diameter changes (%)
Time (min)
d
1 Hz
2 Hz
5 Hz
10 Hz
20 Hz
Area under the curve (10³%.s)

Figure 1: The occurrence and strength of vasoconstriction depends on the photostimulation frequency of pyramidal cells. (a) Representative examples of the voltage responses of a layer II-III pyramidal cell (upper traces light grey to black traces) induced by photostimulations (470 nm, 10 s train, 5 ms pulses) delivered at 1, 2, 5, 10 and 20 Hz (cyan lower traces) and mean spike success rate (middle trace, n= 4 cells from 3 mice). The SEMs envelope the mean traces. The red dashed lines represent a spike success rate of 100%. **(b)** Representative example showing IR-DGC pictures of a layer I penetrating arteriole (1) before a 20 Hz photostimulation, (2) at the maximal diameter decrease, and (3) after 10 minutes of recording. Pial surface is upward. Yellow calipers represent the measured diameters. White dashed lines indicate the initial position of the vessel wall. Scale bar: 25 µm. **(c)** Kinetics of arteriolar diameter changes induced by photostimulation (vertical cyan bars) at 1 Hz (n= 4 arterioles from 3 mice), 2 Hz (n= 10 arterioles from 8 mice), 5 Hz (n= 6 arterioles from 6 mice), 10 Hz (n= 5 arterioles from 5 mice) and 20 Hz (n= 10 arteriole from 9 mice). The SEMs envelope the mean traces. The blue trace represents the kinetics of the diameter changes of the arteriole shown in (b). **(d)** Effects of the different photostimulation frequencies on AUC of vascular responses during 10 min of recording. Data are presented as the individual values and mean ± SEM. * statistically different from 20 Hz stimulation with $p<0.05$.

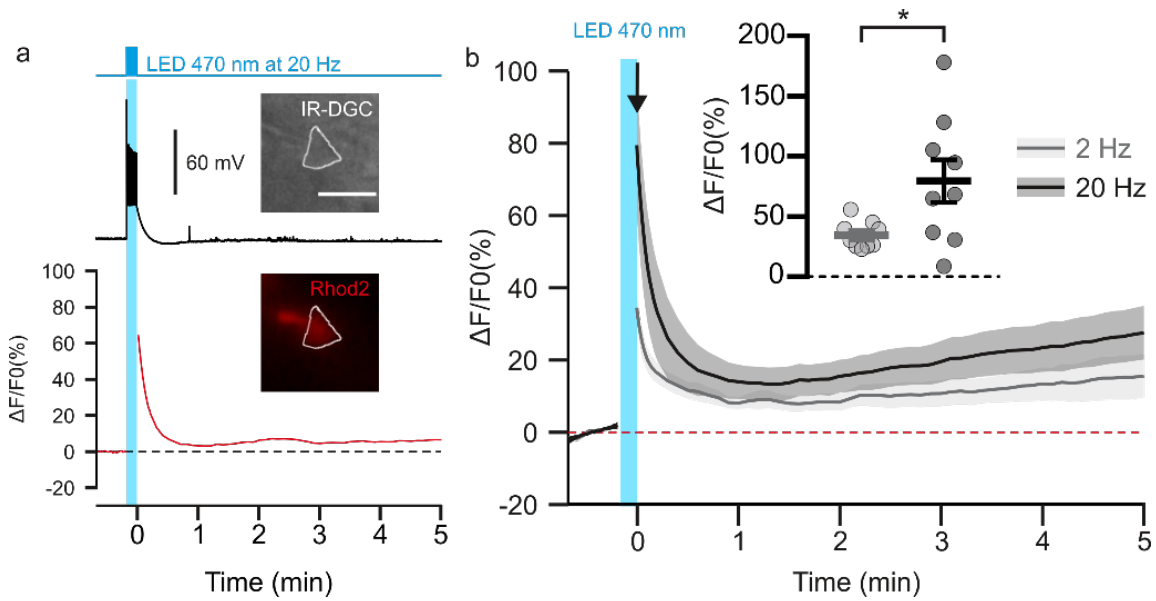

Figure 2: Photostimulation of pyramidal cells elicits a time-locked firing and a frequency-dependent calcium increase. (**a**). Voltage response (top trace) and kinetics of relative fluorescence changes (red bottom trace) induced by photostimulation at 20 Hz. Insets, IR-DGC (top), Rhod2 fluorescence (bottom) pictures of an imaged layer II/III pyramidal cell. The somatic region of interest is outlined in white. Pial surface is upward. Scale bar: 20 µm. **(b)** Mean relative variations of Ca^{2+} fluorescence in response to photostimulation at 2 Hz (grey) and 20 Hz (black). Dashed line represents the baseline. The vertical cyan bar indicates the duration of photostimulation. SEMs envelope the mean traces. Inset, Maximum increase in relative fluorescence changes induced immediately after photostimulation, indicated by the black arrow. The data are shown as the individual values and mean ± SEM. * statistically different with $p < 0.05$.

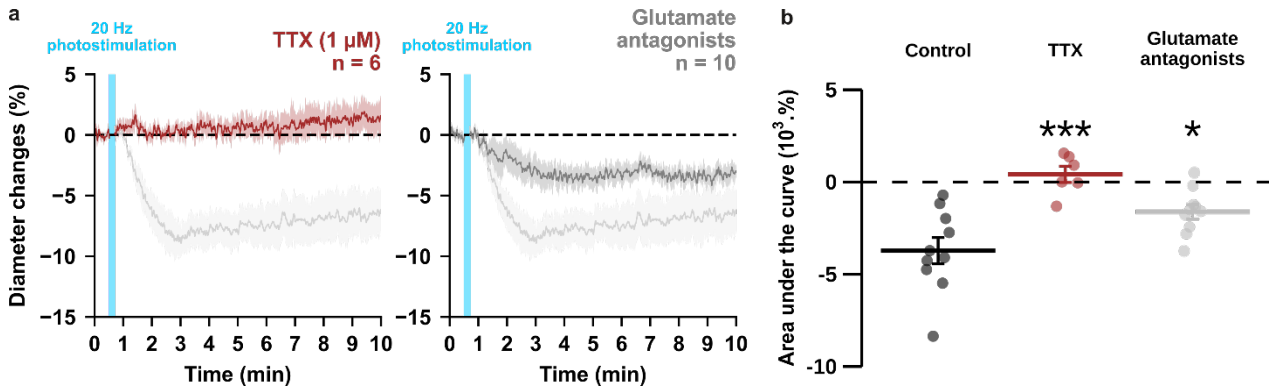

Figure 3: Optogenetically-induced vasoconstriction requires spiking activity and partially glutamatergic transmission. Effect of TTX (1 µM, brown, n= 6 arterioles from 5 mice) and cocktail antagonists of AMPA/kainate (DNQX, 10 µM), NMDA (D-AP5, 50 µM), mGluR1 (LY367385, 100 µM) and mGluR5 (MPEP, 50 µM) receptors (gray, n= 10 arterioles from 6 mice) on **(a)** kinetics and **(b)** magnitude of arteriolar vasoconstriction induced by 20 Hz photostimulation (cyan bar). The SEMs envelope the mean traces. Dashed lines represent the initial diameter. The shadow traces correspond to the kinetics of arteriolar vasoconstriction in control condition. Data are presented as the individual values and mean ± SEM. * and *** statistically different from control condition with $p<0.05$ and $p<0.001$, respectively.

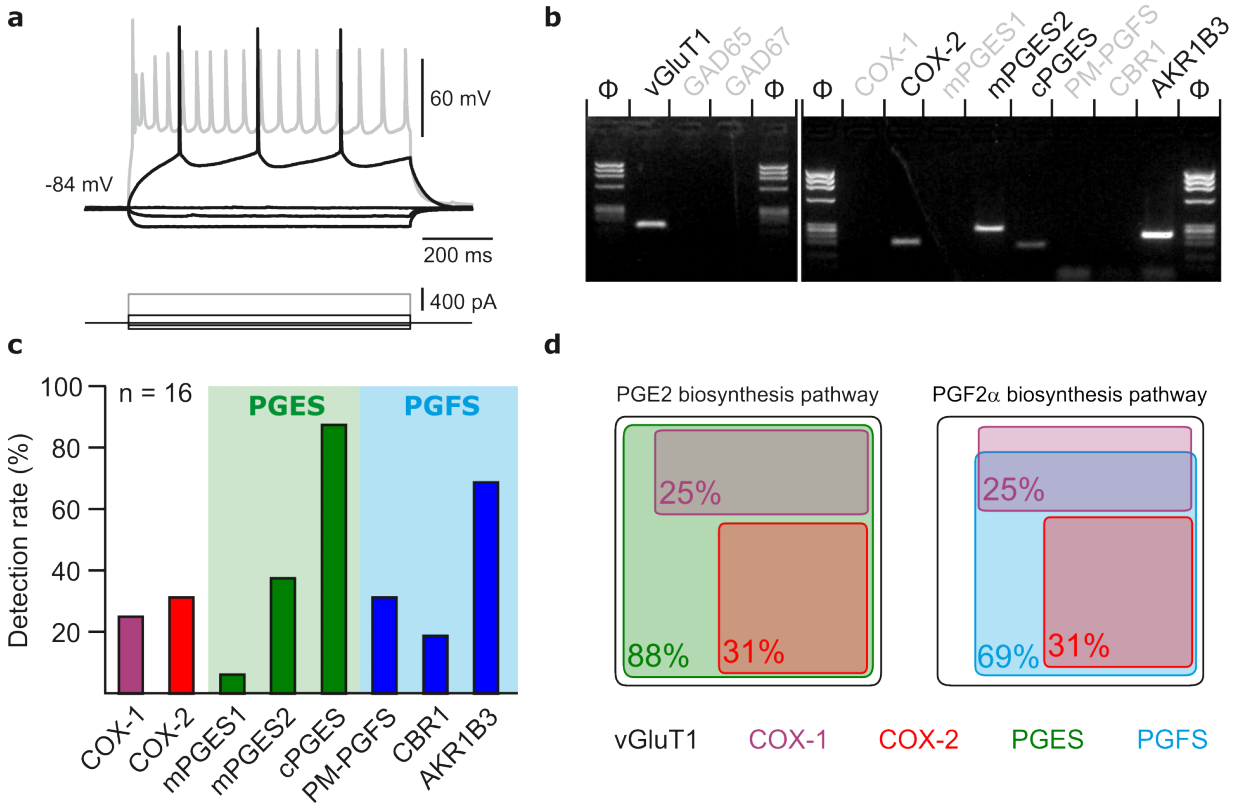

Figure 4: Layer II-III pyramidal cells express PGE2 and PGF2α synthesizing enzymes. (a) Voltage responses of a layer II-III pyramidal cell induced by injection of current (bottom traces). In response to a just-above-threshold current pulse, the neuron fired long-lasting action potentials with little frequency adaptation (middle black trace). Near saturation, it exhibits the pronounced spike amplitude accommodation and marked frequency adaptation characteristic of regular spiking cells (upper grey trace). **(b)** Agarose gel analysis of the scRT-PCR products of the pyramidal cell shown in (**a**) revealing expression of vGluT1, COX-2, mPGES2, cPGES, PM-PGFS and CBR1. Φx174 digested by *HaeIII* (Φ) was used as molecular weight marker **(c)** Histogram summarizing the single-cell detection rate of PGE2 and PGf2α synthesizing enzymes in layer II-III pyramidal cells (n= 16 cells from 6 mice). PGES (green zone) corresponds to mPGES1, mPGES2 and/or cPGES and PGFS (blue zone) to PM-PGFS, CBR1 and/or AKR1B3. **(d)** Co-expression of PGE2 and PGf2α synthesizing enzymes in pyramidal cells. The box size is proportional to the detection rate. Note the absence of co-expression between COX-1 (purple) and COX-2 (red). Co-expression of a PGES (left, green) and a PGFS (right, blue) with COX-1 (up) and COX-2 (bottom).

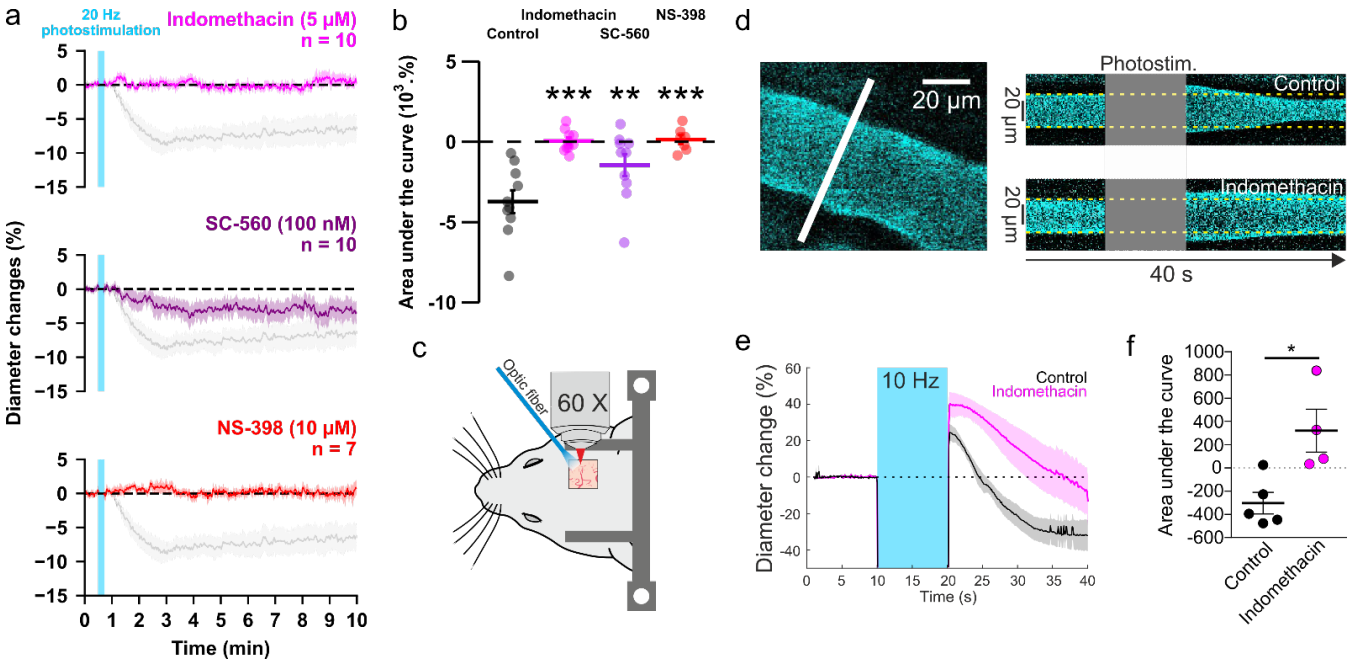

Figure 5: PGE2 mostly derived from COX-2 activity mediates vasoconstriction induced by optogenetically activated pyramidal cells. (a, b) Effects of the COX inhibitors indomethacin (magenta, n= 10 arterioles from 9 mice), SC-560 (purple, n= 10 arterioles from 7 mice) and NS-398 (red, n= 7 arterioles from 6 mice) on kinetics **(a)** and AUC **(b)** of arteriolar vasoconstriction induced by 20 Hz photostimulation (vertical cyan bar). **(c)** Optogenetic stimulation was achieved in vivo with an optic fiber through a chronic cranial window over the barrel cortex. **(d)** Right, diameter change of pial arterioles labeled with fluorescein dextran (i.v) were measured with line-scan crossing the vessel (white line). Left, Representative examples of dilation upon photostimulation (10 Hz, 10 s) under control (top) or indomethacin condition (bottom). **(e)** Diameter changes upon photostimulation under control (black; n = 5 arterioles, 4 mice) or indomethacin (magenta; n = 4 arterioles, 4 mice) conditions. **(f)** Area under the curve of the diameter change in control (black) or indomethacin (magenta) conditions calculated between 20 and 40 s (unpaired, two-tailed Mann Whitney test, * $p<0.05$). The data are shown as the individual values and mean ± SEM. Dashed line represents the baseline. The SEMs envelope the mean traces. The data are shown as the individual values and mean ± SEM. The shadow traces correspond to the control condition. *, ** and *** statistically different from 20 Hz control condition with $p< 0.05$, 0.01 and 0.001, respectively.

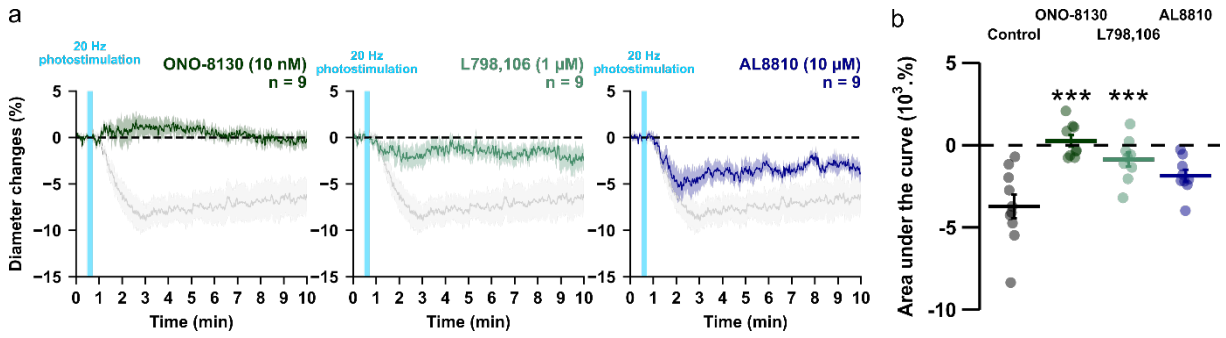

Figure 6: Activation of PGE2 EP1 and EP3 receptors is essential for inducing vasoconstriction triggered by optogenetically activated pyramidal cells. (a, b) Effects of the EP1, EP3 and FP antagonists, ONO-8130 (10 nM, dark green, n= 9 arterioles from 7 mice), L798,106 (1 µM, light green, n= 9 arterioles from 5 mice) and AL8810 (10 µM, dark blue, n= 9 arterioles from 7 mice), respectively, on kinetics **(a)** and AUC **(b)** of arteriolar vasoconstriction induced by 20 Hz photostimulation. Dashed line represents the baseline. The SEMs envelope the mean traces. The data are shown as the individual values and mean ± SEM. The shadow traces correspond to the control condition. *** statistically different from 20 Hz control condition with $p < 0.001$.

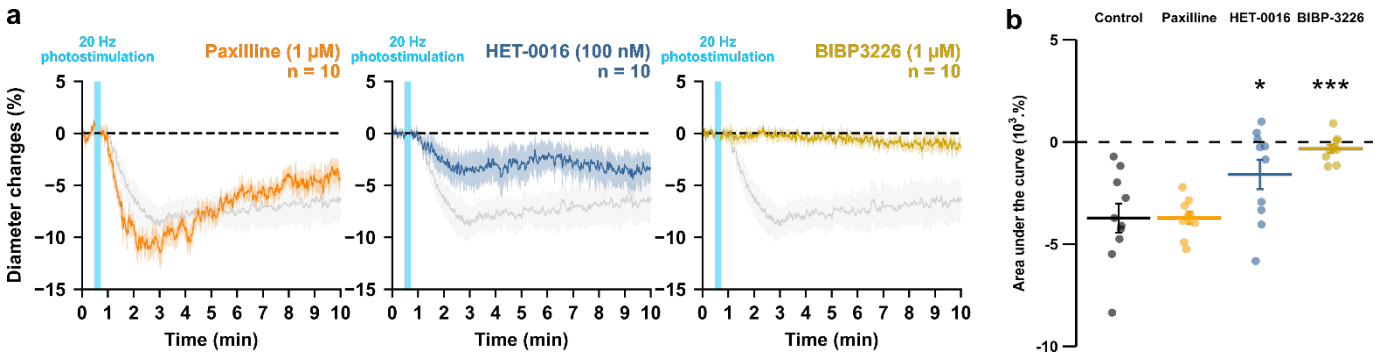

Figure 7: NPY Y1 receptors activation and 20-HETE synthesis mediates the vasoconstriction induced by pyramidal neurons. Effects of paxilline (1 µM, orange, n= 10 arterioles from 6 mice), HET-0016 (100 nM, blue-grey, n= 10 arterioles from 7 mice) and BIBP3226 (1 µM, yellow, n= 10 arterioles from 6 mice) on **(a)** kinetics and **(b)** AUC of arteriolar vasoconstriction induced by 20 Hz photostimulation (vertical blue bar). Dashed line represents the baseline. The SEMs envelope the mean traces. The shadow traces correspond to the control condition. The data are shown as the individual values and mean ± SEM. * and *** statistically different from 20 Hz control condition with $p < 0.05$ and 0.001.

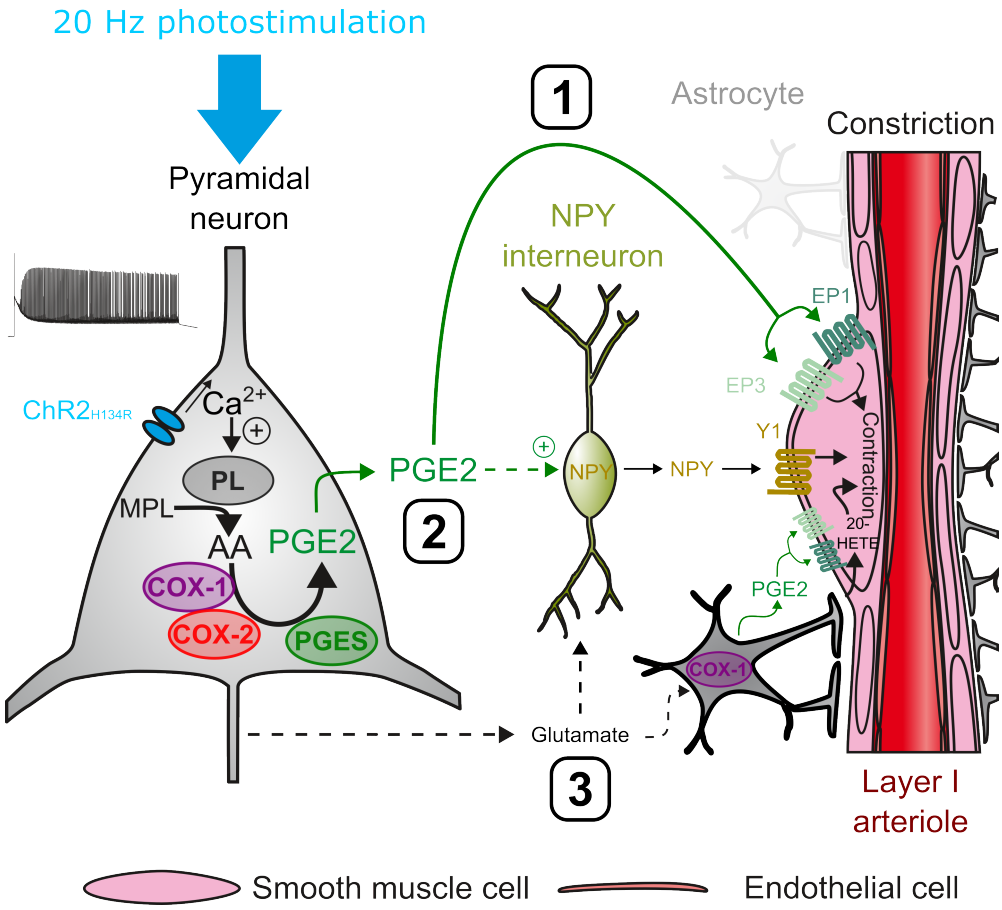

Figure 8: Possible pathways of vasoconstrictions induced by pyramidal neurons. 20 Hz photostimulation induces activation of pyramidal neurons expressing channelrhodopsin-2 ($ChR2_{H134R}$) and elevations of intracellular calcium (Ca^{2+}). Arachidonic acid (AA) is released from membrane phospholipids (MPL) by phospholipases (PL) activated by intracellular Ca^{2+} and metabolized by type-1 and type-2 cyclooxygenases (COX-1 and COX-2) and prostaglandin E2 synthases (PGES) to produce prostaglandin E2 (PGE2). Three possible pathways can be proposed here for the induction arterioles vasoconstriction in layer I: 1) PGE2 released into the extracellular space directly acts on arteriolar EP1 and EP3 receptors to induce constriction of smooth muscle cells. 2) PGE2 activates interneurons and neuropeptide Y (NPY) is released to act on Y1 receptors on smooth muscle cells. 3) Glutamate released by pyramidal cells activates interneurons and astrocytes. Activated astrocytes can induce constriction by the 20-HETE and the COX-1/PGE2 pathways. The three pathways are not exclusive and may act in concert.

References

1. Schmid, F., Barrett, M. J. P., Jenny, P. & Weber, B. Vascular density and distribution in neocortex. Neuroimage 197, 792–805 (2019).

2. Iadecola, C. The Neurovascular Unit Coming of Age: A Journey through Neurovascular Coupling in Health and Disease. *Neuron* **96**, 17–42 (2017).

3. Devor, A. *et al.* Suppressed Neuronal Activity and Concurrent Arteriolar Vasoconstriction May Explain Negative Blood Oxygenation Level-Dependent Signal. *Journal of Neuroscience* **27**, 4452–4459 (2007).

4. Shmuel, A. *et al.* Sustained negative BOLD, blood flow and oxygen consumption response and its coupling to the positive response in the human brain. *Neuron* **36**, 1195–1210 (2002).

5. O'Herron, P. *et al.* Neural correlates of single-vessel haemodynamic responses in vivo. *Nature* **534**, 378–382 (2016).

6. Ma, Y. *et al.* Resting-state hemodynamics are spatiotemporally coupled to synchronized and symmetric neural activity in excitatory neurons. *Proceedings of the National Academy of Sciences* (2016) doi:10.1073/pnas.1525369113.

7. Devor, A. *et al.* Stimulus-Induced Changes in Blood Flow and 2-Deoxyglucose Uptake Dissociate in Ipsilateral Somatosensory Cortex. *Journal of Neuroscience* **28**, 14347–14357 (2008).

8. Uhlirova, H. *et al.* Cell type specificity of neurovascular coupling in cerebral cortex. *Elife* **5**, 1–23 (2016).

9. Farrell, J. S. *et al.* Postictal behavioural impairments are due to a severe prolonged hypoperfusion/ hypoxia event that is COX-2 dependent. (2016) doi:10.7554/eLife.19352.001.

10. Tran, C. H. T., George, A. G., Teskey, G. C. & Gordon, G. R. Seizures elevate gliovascular unit Ca2+ and cause sustained vasoconstriction. *JCI Insight* **5**, (2020).

11. Rungta, R. L., Chaigneau, E., Osmanski, B. F. & Charpak, S. Vascular Compartmentalization of Functional Hyperemia from the Synapse to the Pia. *Neuron* 1–14 (2018) doi:10.1016/j.neuron.2018.06.012.

12. Hill, R. A. *et al.* Regional Blood Flow in the Normal and Ischemic Brain Is Controlled by Arteriolar Smooth Muscle Cell Contractility and Not by Capillary Pericytes. *Neuron* **87**, 95–110 (2015).

13. Hartmann, D. A. *et al.* Brain capillary pericytes exert a substantial but slow influence on blood flow. *Nat Neurosci* **24**, 633–645 (2021).

14. Rungta, R. L. *et al.* vascular arbors in layer II / III somatosensory cortex. *Commun Biol* (2021) doi:10.1038/s42003-021-02382-w.

15. Zhang, D. *et al.* Synaptic-like transmission between neural axons and arteriolar smooth muscle cells drives cerebral neurovascular coupling. *Nat Neurosci* 1–17 (2024) doi:10.1038/s41593-023-01515-0.

16. Cauli, B. *et al.* Cortical GABA interneurons in neurovascular coupling: Relays for subcortical vasoactive pathways. *Journal of Neuroscience* **24**, 8940–8949 (2004).

17. Mulligan, S. J. & MacVicar, B. A. Calcium transients in astrocyte endfeet cause cerebrovascular constrictions. *Nature* **431**, 195–199 (2004).

18. Girouard, H. *et al.* Astrocytic endfoot Ca2+ and BK channels determine both arteriolar dilation and constriction. *Proc Natl Acad Sci U S A* **107**, 3811–3816 (2010).

19. Lecrux, C. *et al.* Pyramidal Neurons Are 'Neurogenic Hubs' in the Neurovascular Coupling Response to Whisker Stimulation. *Journal of Neuroscience* **31**, 9836–9847 (2011).

20. Gordon, G. R. J., Choi, H. B., Rungta, R. L., Ellis-Davies, G. C. R. & MacVicar, B. A. Brain metabolism dictates the polarity of astrocyte control over arterioles. *Nature* **456**, 745–9 (2008).

21. Mishra, A. *et al.* Astrocytes mediate neurovascular signaling to capillary pericytes but not to arterioles. *Nat Neurosci* **19**, 1619–1627 (2016).

22. Lacroix, A. *et al.* COX-2-Derived Prostaglandin E2 Produced by Pyramidal Neurons Contributes to Neurovascular Coupling in the Rodent Cerebral Cortex. *J Neurosci* **35**, 11791–11810 (2015).

23. Rosehart, A. C. *et al.* Prostaglandin E2 Dilates Intracerebral Arterioles When Applied to Capillaries: Implications for Small Vessel Diseases. *Front Aging Neurosci* **13**, 1–11 (2021).

24. Dabertrand, F. *et al.* Prostaglandin E2, a postulated astrocyte-derived neurovascular coupling agent, constricts rather than dilates parenchymal arterioles. *Journal of Cerebral Blood Flow and Metabolism* **33**, 479–482 (2013).

25. Gorski, J. A. *et al.* Cortical excitatory neurons and glia, but not GABAergic neurons, are produced in the Emx1-expressing lineage. *Journal of Neuroscience* **22**, 6309–6314 (2002).

26. Madisen, L. *et al.* A toolbox of Cre-dependent optogenetic transgenic mice for light-induced activation and silencing. *Nat Neurosci* **15**, 793–802 (2012).

27. Lin, J. Y., Lin, M. Z., Steinbach, P. & Tsien, R. Y. Characterization of engineered channelrhodopsin variants with improved properties and kinetics. *Biophys J* **96**, 1803–1814 (2009).

28. Karagiannis, A. *et al.* Classification of NPY-expressing neocortical interneurons. *J Neurosci* **29**, 3642–59 (2009).

29. Chung, D. Y. *et al.* Determinants of Optogenetic Cortical Spreading Depolarizations. *Cerebral Cortex* **29**, 1–12 (2018).

30. Zhou, N., Gordon, G. R. J., Feighan, D. & MacVicar, B. A. Transient swelling, acidification, and mitochondrial depolarization occurs in neurons but not astrocytes during spreading depression. *Cerebral Cortex* **20**, 2614–2624 (2010).

31. Rungta, R. L., Osmanski, B.-F., Boido, D., Tanter, M. & Charpak, S. Light controls cerebral blood flow in naive animals. *Nat Commun* **8**, 14191 (2017).

32. Attwell, D. *et al.* Glial and neuronal control of brain blood flow. *Nature* **468**, 232–43 (2010).

33. Cauli, B. & Hamel, E. Revisiting the role of neurons in neurovascular coupling. *Front Neuroenergetics* **2**, 9 (2010).

34. Smetters, D., Majewska, A. & Yuste, R. Detecting action potentials in neuronal populations with calcium imaging. *Methods: A Companion to Methods in Enzymology* **18**, 215–221 (1999).

35. Tasic, B. *et al.* Adult mouse cortical cell taxonomy revealed by single cell transcriptomics. *Nat Neurosci* **advance on**, 1–37 (2016).

36. Zeisel, A. *et al.* Cell types in the mouse cortex and hippocampus revealed by single-cell RNA-seq. *Science (1979)* **347**, 1138–1142 (2015).

37. Sun, W. *et al.* Glutamate-Dependent Neuroglial Calcium Signaling Differs Between Young and Adult Brain. *Science (1979)* **339**, 197–200 (2013).

38. Zonta, M. *et al.* Neuron-to-astrocyte signaling is central to the dynamic control of brain microcirculation. *Nat Neurosci* **6**, 43–50 (2003).

39. Devienne, G., Le Gac, B., Piquet, J. & Cauli, B. Single Cell Multiplex Reverse Transcription Polymerase Chain Reaction After Patch-Clamp. *Journal of Visualized Experiments* **136**, 1–12 (2018).

40. Sharif, N. A. & Klimko, P. G. Prostaglandin FP receptor antagonists: discovery, pharmacological characterization and therapeutic utility. *Br J Pharmacol* **176**, 1059–1078 (2019).

41. Boie, Y. *et al.* Molecular cloning and characterization of the four rat prostaglandin E 2 prostanoid receptor subtypes. 227–241 (1997).

42. Clasadonte, J. *et al.* Prostaglandin E 2 release from astrocytes triggers gonadotropin-releasing hormone (GnRH) neuron firing via EP2 receptor activation. *Proc Natl Acad Sci U S A* **108**, 16104–16109 (2011).

43. Di Cesare, A., Del Piccolo, P., Zacchetti, D. & Grohovaz, F. EP2 receptor stimulation promotes calcium responses in astrocytes via activation of the adenylyl cyclase pathway. *Cellular and Molecular Life Sciences* **63**, 2546–2553 (2006).

44. Kahn, I. *et al.* Optogenetic drive of neocortical pyramidal neurons generates fMRI signals that are correlated with spiking activity. *Brain Res* **1511**, 33–45 (2013).

45. Scott, N. A. & Murphy, T. H. Hemodynamic responses evoked by neuronal stimulation via channelrhodopsin-2 can be independent of intracortical glutamatergic synaptic transmission. *PLoS One* **7**, 1–10 (2012).

46. Blanco, M., Stern, J. E. & Filosa, J. A. Tone-dependent vascular responses to astrocyte-derived signals. *American journal of physiology.* 2855–2863 (2008) doi:10.1152/ajpheart.91451.2007.

47. Mao, B. Q., Hamzei-Sichani, F., Aronov, D., Froemke, R. C. & Yuste, R. Dynamics of spontaneous activity in neocortical slices. *Neuron* **32**, 883–898 (2001).

48. Niwa, K., Araki, E., Morham, S. G., Ross, M. E. & Iadecola, C. Cyclooxygenase-2 contributes to functional hyperemia in whisker-barrel cortex. *Journal of Neuroscience* **20**, 763–770 (2000).

49. Desai, S., April, H., Nwaneshiudu, C. & Ashby, B. Comparison of agonist-induced internalization of the human EP2 and EP4 prostaglandin receptors: role of the carboxyl terminus in EP4 receptor sequestration. *Mol Pharmacol* **58**, 1279–86 (2000).

50. Kasischke, K. A. *et al.* Two-photon NADH imaging exposes boundaries of oxygen diffusion in cortical vascular supply regions. *Journal of Cerebral Blood Flow and Metabolism* **31**, 68–81 (2011).

51. Yamagata, K., Andreasson, K. I., Kaufmann, W. E., Barnes, C. A. & Worley, P. F. Expression of a Mitogen-Inducible Cyclooxygenase in Brain Neurons : Regulation by Synaptic Activity and Glucocorticoids. *Neuron* **11**, 371–386 (1993).

52. Yamagata, K. *et al.* Coexpression of microsomal-type prostaglandin E synthase with cyclooxygenase-2 in brain endothelial cells of rats during endotoxin-induced fever. *Journal of Neuroscience* **21**, 2669–2677 (2001).

53. Takemiya, T., Matsumura, K. & Yamagata, K. Roles of prostaglandin synthesis in excitotoxic brain diseases. *Neurochem Int* **51**, 112–120 (2007).

54. Takei, S. *et al.* Immunohistochemical demonstration of increased prostaglandin F2α levels in the rat hippocampus following kainic acid-induced seizures. *Neuroscience* **218**, 295–304 (2012).

55. Bao, L. *et al.* Localization of neuropeptide Y Y1 receptors in cerebral blood vessels. *Proc Natl Acad Sci U S A* **94**, 12661–6 (1997).

56. Attwell, D., Mishra, A., Hall, C. N., O'Farrell, F. M. & Dalkara, T. What is a pericyte? *Journal of Cerebral Blood Flow and Metabolism* **36**, 451–455 (2016).

57. Krawchuk, M. B., Ruff, C. F., Yang, X., Ross, S. E. & Vazquez, A. L. Optogenetic assessment of VIP, PV, SOM and NOS inhibitory neuron activity and cerebral blood flow regulation in

mouse somato-sensory cortex. *Journal of Cerebral Blood Flow and Metabolism* **40**, 1427–1440 (2020).

58. Lee, J. *et al.* Opposed hemodynamic responses following increased excitation and parvalbumin-based inhibition. *Journal of Cerebral Blood Flow and Metabolism* (2020) doi:10.1177/0271678X20930831.

59. Zhang, D. Y. & Raichle, M. E. Disease and the brain's dark energy. *Nat Rev Neurol* **6**, 15–28 (2010).

60. Palop, J. J. & Mucke, L. Amyloid-B-induced neuronal dysfunction in Alzheimer's disease: From synapses toward neural networks. *Nat Neurosci* **13**, 812–818 (2010).

61. Thévenaz, P., Ruttimann, U. E. & Unser, M. A pyramid approach to subpixel registration based on intensity. *IEEE Transactions on Image Processing* **7**, 27–41 (1998).

62. R Core Team. R: A Language and Environment for Statistical Computing. Preprint at (2023).

63. Caswell, T. A. *et al.* matplotlib/matplotlib: REL: v3.7.2. (2023) doi:10.5281/ZENODO.8118151.

64. Tournissac, M. *et al.* Cranial window for longitudinal and multimodal imaging of the whole mouse cortex. *Neurophotonics* **9**, 1–13 (2022).